

## Circumnuclear Molecular Gas in Low-redshift Quasars and Matched Star-forming Galaxies

TAKUMA IZUMI,<sup>1,2,\*</sup> JOHN D. SILVERMAN,<sup>3,4</sup> KNUD JAHNKE,<sup>5</sup> ANDREAS SCHULZE,<sup>1</sup> RENYUE CEN,<sup>6</sup> MALTE SCHRAMM,<sup>1</sup> TOHRU NAGAO,<sup>7</sup> LUTZ WISOTZKI,<sup>8</sup> AND WIPHU RUJOPARKAN<sup>3,9,10</sup>

<sup>1</sup>*National Astronomical Observatory of Japan, 2-21-1 Osawa, Mitaka, Tokyo 181-8588, Japan*

<sup>2</sup>*Department of Astronomical Science, The Graduate University for Advanced Studies, SOKENDAI, 2-21-1 Osawa, Mitaka, Tokyo 181-8588, Japan*

<sup>3</sup>*Kavli Institute for the Physics and Mathematics of the Universe (Kavli-IPMU, WPI), The University of Tokyo Institutes for Advanced Study, The University of Tokyo, Kashiwa, Chiba 277-8583, Japan*

<sup>4</sup>*Department of Astronomy, School of Science, The University of Tokyo, 7-3-1 Hongo, Bunkyo-ku, Tokyo 113-0033, Japan*

<sup>5</sup>*Max Planck Institut für Astronomie, Königstuhl 17, D-69117 Heidelberg, Germany*

<sup>6</sup>*Department of Astrophysical Sciences, Princeton University, Princeton, NJ 08544, USA*

<sup>7</sup>*Research Center for Space and Cosmic Evolution, Ehime University, Matsuyama, Ehime 790-8577, Japan*

<sup>8</sup>*Leibniz-Institut für Astrophysik Potsdam (AIP), An der Sternwarte 16, D-14482 Potsdam, Germany*

<sup>9</sup>*Department of Physics, Faculty of Science, Chulalongkorn University, 254 Phayathai Road, Pathumwan, Bangkok 10330, Thailand*

<sup>10</sup>*National Astronomical Research Institute of Thailand, Don Kaeo, Mae Rim, Chiang Mai 50180, Thailand*

(Received April 1, 2020; Revised June 2, 2020; Accepted June 3, 2020)

Submitted to ApJ

### ABSTRACT

A series of gravitational instabilities in a circumnuclear gas disk (CND) are required to trigger gas transport to a central supermassive black hole (SMBH) and ignite Active Galactic Nuclei (AGNs). A test of this scenario is to investigate whether an enhanced molecular gas mass surface density ( $\Sigma_{\text{mol}}$ ) is found in the CND-scale of quasars relative to a comparison sample of inactive galaxies. Here we performed sub-kpc resolution CO(2–1) observations with ALMA of four low-redshift ( $z \sim 0.06$ ), luminous ( $\sim 10^{45} \text{ erg s}^{-1}$ ) quasars with each matched to a different star-forming galaxy, having similar redshift, stellar mass, and star-formation rate. We detected CO(2–1) emission from all quasars, which show diverse morphologies. Contrary to expectations,  $\Sigma_{\text{mol}}$  of the quasar sample, computed from the CO(2–1) luminosity, tends to be smaller than the comparison sample at  $r < 500 \text{ pc}$ ; there is no systematic enhancement of  $\Sigma_{\text{mol}}$  in our quasars. We discuss four possible scenarios that would explain the lower molecular gas content (or CO(2–1) luminosity as an actual observable) at the CND-scale of quasars, i.e., AGN-driven outflows, gas-rich minor mergers, time-delay between the onsets of a starburst-phase and a quasar-phase, and X-ray-dominated region (XDR) effects on the gas chemical abundance and excitation. While not extensively discussed in the literature, XDR effects can have an impact on molecular mass measurements particularly in the vicinity of luminous quasar nuclei; therefore higher resolution molecular gas observations, which are now viable using ALMA, need to be considered.

*Keywords:* galaxies: active — galaxies: ISM — galaxies: evolution — quasars: general — ISM: molecules

### 1. INTRODUCTION

How are supermassive black holes (SMBHs) in galaxies fed? This has been one of the key open questions in astrophysics ever since quasars and active galactic nu-

clei (AGNs) were firmly established to be powered by accretion onto SMBHs. Fueling material needs to lose >99% of its angular momentum to travel from  $\sim 10$  kpc-scale galactic disks all the way down to the central black hole (Lynden-Bell & Rees 1971). Therefore, a specific physical mechanism is required to provide torques that can transport gas to the nuclear region where viscous forces in an accretion disk can then take over (e.g., Balbus & Hawley 1998).

Corresponding author: Takuma Izumi  
 takuma.izumi@nao.ac.jp

\* NAOJ Fellow

In principle, major gas-rich galaxy mergers (such as observed as ultra-luminous infrared galaxies = ULIRGs, [Sanders & Mirabel 1996](#)) could provide one such mechanism, generating torques leading to massive gas inflows (e.g., [Hernquist 1989](#); [Di Matteo et al. 2005](#); [Hopkins et al. 2006, 2008](#)). Recent high resolution and/or high sensitivity observations indeed show enhanced AGN fraction in major merger systems ([Ellison et al. 2011](#); [Silverman et al. 2011](#); [Koss et al. 2018](#); [Goulding et al. 2018](#)), which is particularly the case for dust-reddened quasars (e.g., [Urrutia et al. 2008](#)). While capable of triggering AGN, major mergers are not likely the *dominant* mechanism for fueling most SMBHs out to  $z \sim 2$  (e.g., [Cisternas et al. 2011](#); [Schawinski et al. 2012](#); [Kocevski et al. 2012](#); [Mechtley et al. 2016](#)). It appears that mergers account for about  $\sim 20\%$  of all AGN activity ([Silverman et al. 2011](#)).

For nearby low-luminosity AGNs (i.e., Seyfert-class; nuclear bolometric luminosity  $\lesssim 10^{44}$  erg s $^{-1}$ ), secular processes, induced by for example, a barred gravitational potential, galaxy-galaxy interaction (e.g., [Shlosman et al. 1990](#); [Kormendy & Kennicutt 2004](#); [Hopkins & Hernquist 2006](#)), or minor mergers (e.g., [Mihos & Hernquist 1994](#); [Taniguchi 1999](#); [Kaviraj 2014](#)), may be sufficient to redistribute gas in the galaxy and transport angular momentum outward. Recent multi-scale hydrodynamical simulations (e.g., [Hopkins & Quataert 2010](#)) predict that such gravitational instabilities are also the mechanism for gas transport in luminous AGNs (i.e., quasar-class) that dominate black hole growth. The simulations show that when the gas mass surface density is sufficiently high in the central  $\sim$  several  $\times 100$  pc region of a gaseous *circumnuclear disk* (CND), a series of instabilities occur, which could then reach gas down to sub-pc scales. In this picture, *black hole accretion generally takes place if sufficient gas is deposited at the CND-scale irrespective of the mechanism*.

How much gas is deposited at the CND-scale and on what timescale in the hosts of luminous quasars are currently unanswered questions. These most likely further depend on redshift, mass, and local environment. In nearby Seyfert galaxies, [Izumi et al. \(2016a\)](#) found a positive correlation between dense molecular gas mass of CND and AGN luminosity, supporting the importance of circumnuclear gas amount in AGN fueling. For luminous quasars at  $z \gtrsim 0.1$ , molecular gas observations have been limited in resolution to  $\gtrsim$  a few arcsec ( $>$  kpc) thus far ([Scoville et al. 2003](#); [Evans et al. 2001, 2006](#); [Shangguan et al. 2020](#)), probing only the total gas content.

Now the Atacama Large Millimeter/submillimeter Array (ALMA) permits us to spatially resolve the central sub-kpc of such quasar-host galaxies. According to the simulations (e.g., [Hopkins & Quataert 2010](#)), there should be a threshold in the nuclear gas density, above

which self-gravitating instabilities can form, and below which inflows essentially do not exist. As a first step to test this scenario, here we study whether significantly higher gas mass surface densities, which are the key parameter determining gravitational instability, are observed by ALMA at the CND-scale in luminous quasars (accretion rate  $> 10\%$  of the Eddington-limited value) relative to comparison galaxies without AGN. Note that the actual accretion rate should fluctuate strongly (e.g., [Novak et al. 2011](#); [Schawinski et al. 2015](#)): an observed intermediate accretion rate could either be due to a genuinely low inflow rate, or just to a temporally fluctuated low accretion rate for a very high inflow rate. This ambiguity can be reduced in a statistical sense when we observe more and more luminous quasars.

This effort is organized as follows. In Section 2, we describe the details of our sample selection and ALMA observations. The observed properties are presented in Section 3. We discuss hypothesized differences in CND-scale gas mass surface density between quasars and comparison galaxies in Section 4. Our conclusions are summarized in Section 5. Throughout this paper, we adopt the concordant cosmological parameters  $H_0 = 70$  km s $^{-1}$  Mpc $^{-1}$ ,  $\Omega_M = 0.3$ , and  $\Omega_\Lambda = 0.7$ .

## 2. DATA DESCRIPTION

### 2.1. Sample Selection

To test the above hypothesis, we selected quasars and inactive galaxies, matched in redshift, stellar mass ( $M_\star$ ), and global star formation rate (SFR) (Figure 1; Table 1). This leaves central gas surface density and AGN activity as prime parameters: a positive correlation between these therefore implies a causation. We initially selected  $N = 5$  quasar-galaxy pairs for this purpose, but later realized that one pair is not well matched in SFR actually. Hence, we excluded that pair from our work, which leaves  $N = 4$  pairs (see Appendix for details of the excluded pair). With this sample size, we can rule out the possibility that all quasars have higher gas surface density than galaxies solely by chance at a coincidence level of  $\sim 94\%$  (random probability =  $0.5^N = 6\%$ ).

For the quasar sample, we selected nearby ( $z < 0.08$ ), massive (black hole mass  $M_{\text{BH}} > 10^{7.7} M_\odot$  measured with the H $\beta$ -based single epoch method, [Vestergaard & Peterson 2006](#)), high-accretion type-1 objects from the Palomar-Green (PG) quasar sample ([Schmidt & Green 1983](#)) and the Hamburg/ESO (HE) Survey quasar sample ([Wisotzki et al. 2000](#); [Schulze & Wisotzki 2010](#)) with declination  $\delta < 15^\circ$ . Their quasar bolometric luminosities ( $L_{\text{Bol}}$ ) are  $\sim 10^{45}$  erg s $^{-1}$ , which roughly correspond to the knee of the quasar luminosity function at this redshift range (e.g., [Shankar et al. 2009](#); [Schulze et al. 2009](#)) and allow us to better avoid the aforementioned degeneracy due to time-fluctuation. Their  $M_\star$  are inferred from the local mass relation between SMBH and their host galaxy ([Kormendy & Ho 2013](#)). We used the far-

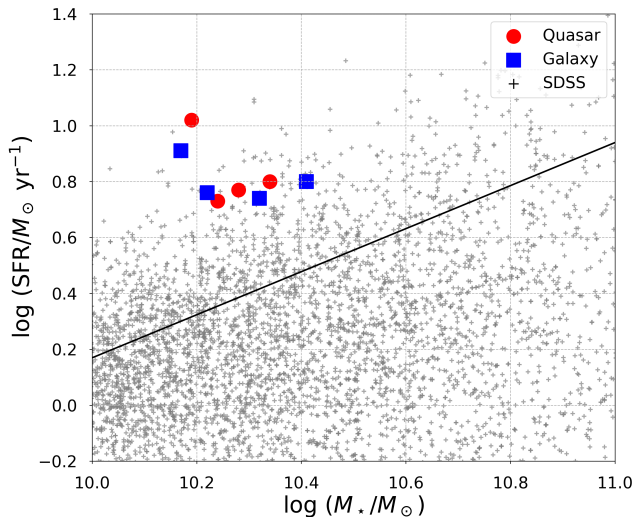


**Figure 1.** Location of our quasar and comparison galaxy samples in the stellar mass ( $M_*$ ) – star-formation rate (SFR) plane. The red circles show the quasar sample while the blue squares show the comparison sample matched in  $M_*$ , SFR, and  $z$ , respectively. The background gray points indicate the parent SDSS galaxies at  $0.05 < z < 0.08$ , which we used to draw the comparison sample. The black line indicates the  $z \sim 0$  star-forming main sequence (Elbaz et al. 2007).

infrared luminosity estimated from  $L_{\text{Bol}}$  (Netzer et al. 2007; Rosario et al. 2013) to compute SFRs of our quasars based on the Kennicutt-Schmidt relation (e.g., Kennicutt & Evans 2012). Note that these quasars were originally ultraviolet-selected, hence were not biased by the amount of gas and dust in their host galaxies.

We constructed a comparison sample of inactive galaxies (in terms of quasar activity) selected from the SDSS DR10 MPA-JHU galaxy catalog (Eisenstein et al. 2011; Brinchmann et al. 2004), which is matched to the quasar sample in fundamental parameters – except SMBH accretion rate (Figure 1). Their  $M_*$  values are computed by SED fits to photometry following Kauffmann et al. (2003). SFRs are measured with  $\text{H}\alpha$  line emission for the SDSS galaxies (Brinchmann et al. 2004). The constructed  $N = 4$  pairs are exhibited in Figure 2.

## 2.2. ALMA Observations

We observed the redshifted  $^{12}\text{CO}(2-1)$  line (rest frequency  $\nu_{\text{rest}} = 230.5380$  GHz) and its underlying continuum emission (at the rest frame wavelength  $\lambda_{\text{rest}} \sim 1.3$  mm) towards our targets with ALMA, during Cycle 4 using the Band 6 receiver (project ID: #2015.1.00872.S). As  $\text{CO}(2-1)/\text{CO}(1-0)$  line ratio (or excitation) is widely measured in various kinds of galaxies (see more details in § 4), we can compute molecular masses by using this  $\text{CO}(2-1)$  line as a surrogate of the ground-transition  $\text{CO}(1-0)$  line, while easily acquiring higher angular res-

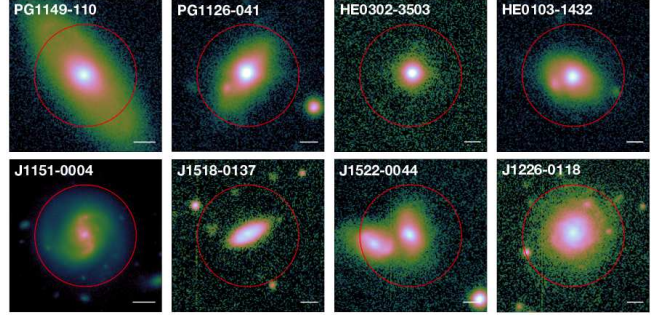


**Figure 2.** A gallery of our target quasars and inactive galaxies taken with the Subaru Hyper Suprime-Cam (J1151-0004;  $R$ -band) and ESO 2.2m Telescope WFI (the rest; ESO843 filter  $\sim V$ -band). Each panel shows  $0.6'$  region centered on each nucleus, which are recorded in *GAIA* or SDSS database. The horizontal white scale bars correspond to 5 kpc length, and the red circles denote the nominal field of view of our ALMA observations ( $\sim 24''$ ), respectively.

olutions than cases of lower frequency  $\text{CO}(1-0)$  observations. In total 37–43 antennas were used with the baseline ranging from 15.1 m to 1.1 km (0.7 km in some cases), resulting in a nominal maximum recoverable scale of  $\sim 10''$ . The reduction and calibration were done with CASA version 4.7 (McMullin et al. 2007) in the standard manner. Continuum emission was subtracted in the  $uv$ -plane before making line cubes.

All of the images presented in this paper were reconstructed using the task `clean` with the natural weighting to enhance sensitivities, resulting in synthesized beam sizes of  $\sim 0.34''$ – $0.74''$  (major axes). The achieved  $1\sigma$  sensitivities are  $0.26$ – $0.41$  mJy beam $^{-1}$  (quasars) and  $0.16$ – $0.56$  mJy beam $^{-1}$  (comparison galaxies), respectively, for the  $\text{CO}(2-1)$  cubes: here we set the frequency resolution ( $df$ ) to 62.5 MHz (velocity resolution  $dV \simeq 86$  km s $^{-1}$ ) for quasars, whereas  $df = 31.25$  MHz ( $dV \simeq 43$  km s $^{-1}$ ) for comparison galaxies, after finding that the lines are relatively fainter in the former (but with broader widths; see § 3). Further details can be found in Table 2. Note that on-source integration times were significantly shorter for the quasars (2–5 min) than for the comparison galaxies (4–12.5 min). The 10% absolute flux uncertainty, according to the ALMA proposer’s guide, is not included unless mentioned otherwise.

## 3. RESULTS

### 3.1. $\text{CO}(2-1)$ emission

Figure 3 shows the spatial distribution of the  $\text{CO}(2-1)$  line and underlying 1.3 mm continuum emission within the central  $3''$  region of our sample. Note that the coordinates of their centers are tied to the *Gaia* reference system except for J1151–0004, J1522–0044, and J1226–0118 (SDSS system). Their  $\text{CO}(2-1)$  line spec-

**Table 1.** Target quasars and comparison inactive galaxies

Name	R.A. (ICRS)	Decl. (ICRS)	$z_{\text{opt}}$	Scale (kpc/‘‘)	$\log \left( \frac{M_{\text{BH}}}{M_{\odot}} \right)$	$\log \left( \frac{L_{\text{bol}}}{\text{erg/s}} \right)$	$\log \left( \frac{M_{\star}}{M_{\odot}} \right)$	$\log \left( \frac{SFR}{M_{\odot}/\text{yr}} \right)$
PG1149–110	11:52:03.550	–11:22:24.09	0.049	0.96	7.92	45.1	10.34	0.80
PG1126–041	11:29:16.729	–04:24:07.25	0.060	1.17	7.75	45.3	10.19	1.02
HE0302–3503	03:04:26.924	–34:52:07.66	0.066	1.27	7.86	45.0	10.28	0.77
HE0103–1432	01:05:38.792	–14:16:13.58	0.066	1.27	7.81	45.0	10.24	0.73
J1151–0004	11:51:30.954	–00:04:39.93	0.048	0.93	–	–	10.41	0.80
J1518–0137	15:18:34.689	–01:37:43.83	0.063	1.20	–	–	10.17	0.91
J1522–0044	15:22:24.740	–00:44:04.58	0.067	1.28	–	–	10.32	0.74
J1226–0118	12:26:46.972	–01:18:54.13	0.062	1.20	–	–	10.22	0.76

NOTE—Top four objects are the target quasars and the bottom four are the comparison galaxies, which are listed in a paired order (e.g., PG1149–110 and J1151–0004). Their coordinates are tied to the *Gaia* reference system except for J1151–0004, J1522–0044, and J1226–0118 (SDSS system).

tra are presented in Figure 4, which are used to determine the CO-based redshifts ( $z_{\text{CO}}$ ). The line emission was successfully detected in all of the targets and the line-emitting regions are spatially resolved in these global integrated intensity maps. We made these CO(2–1) maps (Figure 3) by integrating velocity channels over the line profiles. For the case of PG1149–110, in which the CO(2–1) line profile is not clear due to the modest signal-to-noise (S/N) ratio, we integrated over a velocity range of  $\sim -400$  to  $+400$  km s $^{-1}$ .

As for the quasar sample, line widths are broad with full-width at zero intensity (FWZI)  $\sim 400 - 500$  km s $^{-1}$ , which is consistent with the previous single dish-based CO observations toward optically-luminous PG/HE quasars ( $M_B < -20$  mag, [Bertram et al. 2007](#)). We also found that the line spectrum of PG1126–041, and likely that of PG1149–110, show double-horn profiles characteristic of a rotating CND. Recently, Atacama Compact Array (ACA) observations of CO(2–1) emission by [Shangguan et al. \(2020\)](#) also reported a double-horn like profile for PG1126–041 but on a larger scale ( $\sim 6''$  resolution).

The CO line width is generally broader in the quasar sample than in the comparison sample. A line profile can be broader if the inclination angle of a system becomes higher, but we would not expect in terms of chance probability that all of our quasars have higher inclination angles than their matched galaxies. Hence, the broader line width would indicate higher gas rotation velocity and/or velocity dispersion in the quasar sample than in the comparison sample. One potential cause of a broader profile is a molecular outflow. However, it is hard to tell whether there are indications of outflows in our quasar spectra given the modest S/N ratios. Another possibility is that the quasars have larger enclosed mass (BH + stellar + gas) than comparison galaxies. In this case, the quasars may be in a later evolution-

ary phase than the star-forming comparison galaxies. A relevant discussion can be found in § 4.

The morphology of the gas distribution is diverse with spiral-arm-like features (PG1126–041 and J1518–0137), bar- or edge-on disk-like structures (HE0103–1432 and J1226–0118), and face-on disk-like structures (HE0302–3503 and J1522–0044). In each case, we found that essentially all of the CO(2–1) emission we have recovered emerges from the central  $\sim$ a few kpc around the nuclei. Hereafter, we will focus on this small scale ( $\lesssim 1''$ ) that is much smaller than our maximum recoverable scales (MRS), i.e., missing flux should not be an issue. This may start not to hold when we investigate larger scales, e.g., that is traced by the ACA (aperture  $\sim 6''$ , see recent observations toward PG quasars in [Shangguan et al. 2020](#)). Hence we do not directly compare our results at this time with those of [Shangguan et al. \(2020\)](#).

Following [Solomon & Vanden Bout \(2005\)](#) we computed the CO(2–1) line luminosity ( $L'_{\text{CO}(2-1)}$ ) as

$$\left( \frac{L'_{\text{CO}(2-1)}}{\text{K km s}^{-1} \text{ pc}^2} \right) = 3.25 \times 10^7 \left( \frac{S_{\text{CO}(2-1)} \Delta V}{\text{Jy km s}^{-1}} \right) \left( \frac{\nu_{\text{rest}}}{\text{GHz}} \right)^{-2} \left( \frac{D_L}{\text{Mpc}} \right)^2 (1+z)^{-1}, \quad (1)$$

where  $S_{\text{CO}(2-1)} \Delta V$  is the integrated line flux and  $D_L$  is the luminosity distance to the object. We first convolved the aperture of individual data cubes to the largest one among our full sample in physical scale, i.e.,  $\sim 700$  pc (J1151–0004). This sufficiently covers the typical CND-scale, as well as is roughly comparable to the spatial scale at which simulations (e.g., [Hopkins & Quataert 2010](#)) start to see elevated gas surface density in quasars. The CO measurements within a central aperture for each object are summarized in Table 3. CO line luminosities

are  $\sim (2 - 7) \times 10^7$  K km s $^{-1}$  pc $^2$  for the quasar sample and  $\sim (3 - 19) \times 10^7$  K km s $^{-1}$  pc $^2$  for the comparison sample, respectively. Except for PG1126–041, all of our quasars show fainter  $L'_{\text{CO}(2-1)}$  than the matched galaxies (see § 4 for further discussion). We stress that it is impossible to estimate how much of the total flux is concentrated at this small scale as there is no single dish CO(2–1) data available except for PG1126–041: in this particular case we found that  $\sim 12\%$  of the total flux measured with the IRAM 30 m telescope (14.9 Jy km s $^{-1}$ , Bertram et al. 2007) originates from the central 700 pc.

### 3.2. Comments on J1151–0004

As shown in Figures 3 or 4, one comparison galaxy J1151–0004 is exceptionally bright in CO(2–1) emission ( $L'_{\text{CO}(2-1)} \simeq 2 \times 10^8$  K km s $^{-1}$  pc $^2$  at the central 700 pc). This galaxy was matched to the quasar PG1149–110, which shows much fainter CO(2–1) emission (Table 3). The  $L'_{\text{CO}(2-1)}$  of J1151–0004 is very high even among the comparison sample as well.

For a possible explanation of this high  $L'_{\text{CO}(2-1)}$ , we first considered that J1151–0004 hosts a significant level of dust-obscured star-formation, which is undetectable with SDSS. We further investigated the mid-infrared (MIR) photometric data of our comparison sample obtained by *Wide-field Infrared Survey Explorer* (*WISE*; Wright et al. 2010), which is sensitive to dust-obscured activity. An estimated 8–1000  $\mu\text{m}$  total IR luminosity ( $L_{\text{TIR}}$ ), using a tight correlation between  $L_{\text{TIR}}$  and  $W3$  band luminosity (Cluver et al. 2017), is  $L_{\text{TIR}} = 7 \times 10^{10} L_{\odot}$  ( $W3$  magnitude = 8.35 mag) for the case of J1151–0004. This corresponds to  $\text{SFR} \sim 10 M_{\odot} \text{ yr}^{-1}$  (Murphy et al. 2011), which is still comparable to the SDSS-based unobscured SFR (Table 1). Moreover, the rest of the comparison galaxy sample also shows similar TIR-based SFR ( $\sim 7 - 13 M_{\odot} \text{ yr}^{-1}$ ). Hence, the dust-obscured star-formation of J1151–0004 does not stand out among the comparison sample. Note that this measurement cannot be performed for the quasar sample as warm dust heated by the quasars themselves will dominate their *WISE* fluxes. We also considered the presence of a dust-obscured AGN as it may be hosted in a gas-rich galaxy. To briefly test this scenario, we measured *WISE* colors of our samples. We found that J1151–0004 has consistent *WISE* colors ([4.6]–[12.0] vs [3.4]–[4.6] plane; Figure 5) with the rest of the galaxy sample, while our quasars show typical colors for quasars, indeed. Taking these into consideration, we suppose that J1151–0004 is genuinely a star-forming galaxy that is exceptionally bright in CO(2–1). Any comparison with the matched quasar should be treated with care.

### 3.3. Continuum emission

We detected  $\lambda_{\text{rest}} \simeq 1.3$  mm continuum emission significantly ( $> 3\sigma$ ) in PG1149–110, J1151–0004,

and HE0103–1432, as well as marginally ( $\sim 3\sigma$ ) in PG1126–041 (Figure 3). The nominal detection rate is 3 times higher for the quasar sample than for the comparison sample despite the shorter integration times for the former sample. The sizes of the continuum-emitting regions ( $\lesssim 0''.5$ ) are smaller than the CO-emitting regions, i.e., more centrally concentrated. These likely imply a significant contribution of quasar-induced emission to the submillimeter continuum emission, either as additional heating to the thermal dust emission or as non-thermal synchrotron emission. Note that in the nearby luminous Seyfert galaxy NGC 1068, it is claimed that about half of ALMA Band 6 continuum flux measured around the nucleus is of non-thermal origin (García-Burillo et al. 2014). As comparably high resolution radio-to-submillimeter continuum data is sparse for our targets, we do not perform detailed analysis to further reveal the nature of the Band 6 continuum emission.

### 3.4. Estimates of molecular gas mass

Molecular gas mass ( $M_{\text{mol}}$ ) is conventionally determined from CO(1–0) line luminosity  $L'_{\text{CO}(1-0)}$  by using a CO-to-molecular mass conversion factor  $\alpha_{\text{CO}}$  (Bolatto et al. 2013, and references therein). Note that this molecular mass includes He and heavier elements in addition to H<sub>2</sub>. To compute  $M_{\text{mol}}$ , we first need to convert  $L'_{\text{CO}(2-1)}$  to  $L'_{\text{CO}(1-0)}$ . We here assume  $J = 2-1$  to 1–0 CO brightness temperature ratio  $R_{21} = 1$ , which is the case of optically-thick and fully thermalized excitation. A value of  $R_{21} \sim 1$  has been observed in the central regions of nearby star-forming galaxies (e.g., Bayet et al. 2004; Sandstrom et al. 2013), IR-luminous galaxies (e.g., Papadopoulos et al. 2012; Saito et al. 2017), Seyfert galaxies (e.g., Mashian et al. 2015), as well as in a global scale of high redshift submillimeter galaxies and luminous quasar host galaxies (Carilli & Walter 2013). On the other hand, a lower  $R_{21}$  of  $\sim 0.5 - 0.8$  is frequently observed in >kpc scale galactic disks (e.g., Leroy et al. 2013; Saintonge et al. 2017). The latter value is also found for HE/PG quasars when observed at >a few kpc resolutions (Bertram et al. 2007; Husemann et al. 2017; Shangguan et al. 2020). Since we now investigate the central sub-kpc regions, however, we adopt  $R_{21} = 1$  throughout this work.

Sandstrom et al. (2013) investigated 26 nearby star-forming galaxies and obtained 782 individual determinations of  $\alpha_{\text{CO}}$  coupled with a gas-to-dust ratio, after spatially-resolving the targets at some level. As an average for all of their values without weighting,  $\alpha_{\text{CO}} = 2.6 M_{\odot} \text{ pc}^{-2} (\text{K km s}^{-1})^{-1}$  is recommended, which has 0.4 dex standard deviation. This is somewhat lower than the Milky Way value of  $4.3 M_{\odot} \text{ pc}^{-2} (\text{K km s}^{-1})^{-1}$  (Bolatto et al. 2013), and is not strongly dependent on metallicity of galaxies as long as that metallicity is comparable to, or higher than, the solar value. In the central  $\lesssim$ kpc regions of galaxies, Sandstrom et al. (2013)

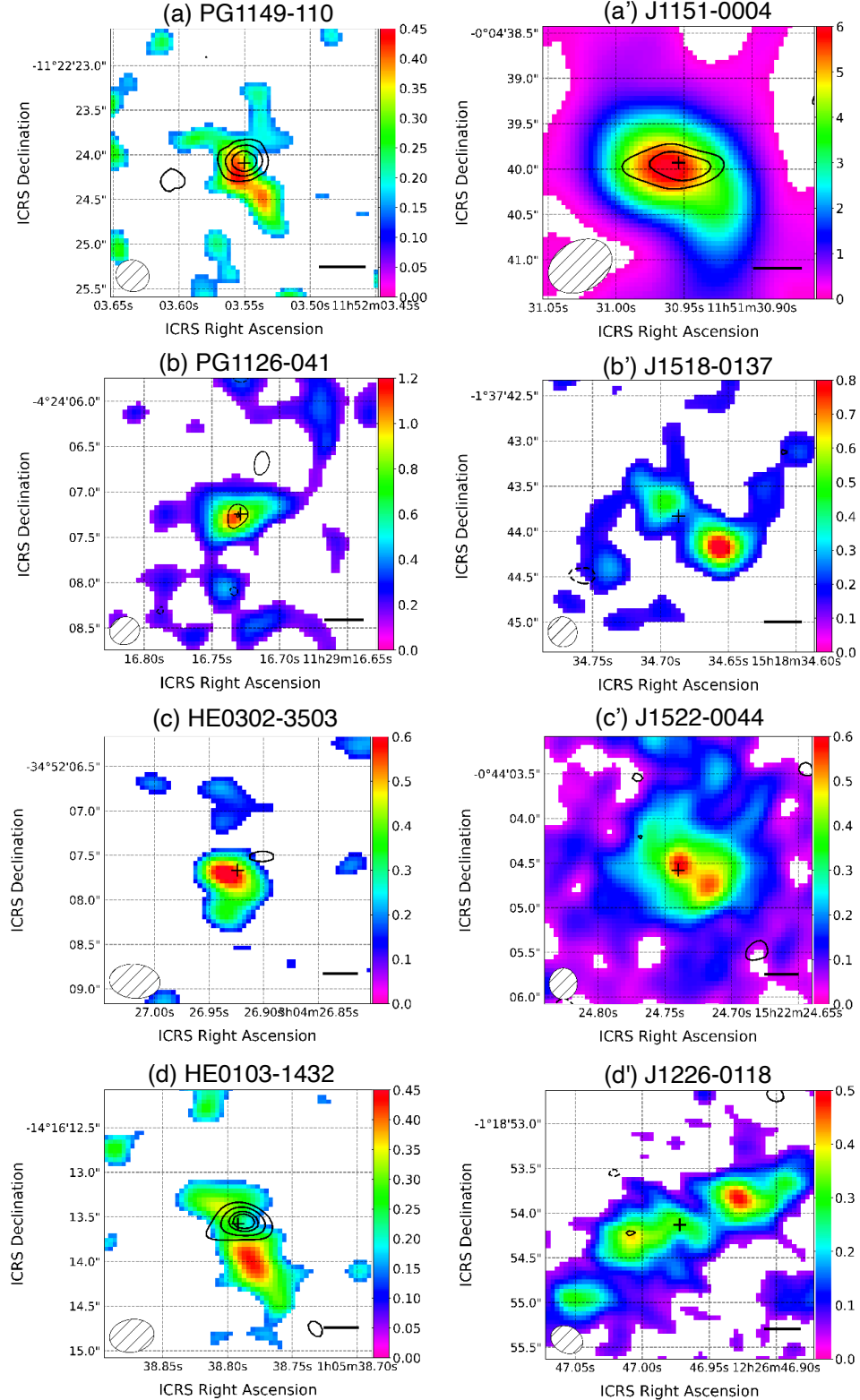


**Figure 3.** Velocity-integrated intensity maps of the CO(2–1) line emission (in units of  $\text{Jy beam}^{-1} \text{ km s}^{-1}$ ) of the central  $3''$  region of our quasars (left column) and comparison galaxies (matched by letter; right column). The  $1\sigma$  sensitivity are  $(0.099, 0.092)$ ,  $(0.092, 0.039)$ ,  $(0.084, 0.023)$ , and  $(0.090, 0.031)$   $\text{Jy beam}^{-1} \text{ km s}^{-1}$  for  $(\text{a}, \text{a}')$ ,  $(\text{b}, \text{b}')$ ,  $(\text{c}, \text{c}')$ , and  $(\text{d}, \text{d}')$ , respectively. The CO(2–1) maps start at  $1.5\sigma$  level to enhance the clarity. The central plus signs indicate the location of the quasar nuclei or galactic centers recorded in the *Gaia* or SDSS database. The contours indicate the continuum emission drawn at  $-3, 3, 4, 5$ , and  $7\sigma$  (see Table 2 for  $1\sigma$  values). The black horizontal bars correspond to 500 pc.

**Table 2.** Descriptions of the CO(2–1) cubes and continuum maps

Name	Beam size (CO: " $\times$ ", $^{\circ}$ )	Beam size (Cont.: " $\times$ ", $^{\circ}$ )	$1\sigma$ (CO) (mJy/beam)	$z_{\text{CO}}$	$1\sigma$ (Cont.) ( $\mu\text{Jy}/\text{beam}$ )
PG1149–110	$0.38 \times 0.35$ , 69.5	$0.34 \times 0.32$ , 73.3	0.41	0.0491	56.9
PG1126–041	$0.34 \times 0.30$ , –65.3	$0.32 \times 0.29$ , –65.6	0.32	0.0603	47.3
HE0302–3503	$0.57 \times 0.39$ , 85.3	$0.54 \times 0.37$ , 83.2	0.31	0.0656	38.7
HE0103–1432	$0.50 \times 0.37$ , –80.9	$0.45 \times 0.34$ , –84.6	0.26	0.0669	42.8
J1151–0004	$0.74 \times 0.55$ , –61.0	$0.72 \times 0.52$ , –59.5	0.56	0.0477	44.3
J1518–0137	$0.33 \times 0.32$ , 23.8	$0.33 \times 0.31$ , 23.5	0.22	0.0628	26.2
J1522–0044	$0.35 \times 0.31$ , 0.1	$0.33 \times 0.31$ , 2.9	0.16	0.0669	17.3
J1226–0118	$0.37 \times 0.30$ , 62.8	$0.34 \times 0.29$ , 64.2	0.21	0.0625	22.5

NOTE—  $1\sigma$  sensitivities are determined in channels free of line emission extracted at the positions of the nuclei (CO cubes) and areas free of emission (continuum maps), respectively. The CO-based redshift ( $z_{\text{CO}}$ ) of each object was determined from an averaged frequency of channels containing  $> 2\sigma$  emission (see also Figure 4).

**Table 3.** CO line measurement and molecular gas mass

Name	$S_{\text{CO}(2-1)}$ (Jy km s $^{-1}$ )	$L'_{\text{CO}(2-1)}$ ( $10^7$ K km/s pc $^2$ )	$M_{\text{mol}}$ ( $10^7 M_{\odot}$ )	$S_{\text{CO}(2-1)}$ (Jy km s $^{-1}$ )	$L'_{\text{CO}(2-1)}$ ( $10^7$ K km/s pc $^2$ )	$M_{\text{mol}}$ ( $10^7 M_{\odot}$ )	$f_{0.7/2.0}$ (%)
	$\theta = 700$ pc			$\theta = 2$ kpc			
PG1149–110	$0.74 \pm 0.21$	$2.1 \pm 0.6$	2.7	$1.66 \pm 0.39$	$4.6 \pm 1.1$	6.0	$45 \pm 16$
PG1126–041	$1.73 \pm 0.21$	$7.3 \pm 0.9$	9.5	$2.76 \pm 0.44$	$11.6 \pm 1.9$	15.1	$63 \pm 13$
HE0302–3503	$0.67 \pm 0.12$	$3.4 \pm 0.6$	4.4	$0.89 \pm 0.15$	$4.5 \pm 0.7$	5.9	$75 \pm 18$
HE0103–1432	$0.42 \pm 0.10$	$2.2 \pm 0.5$	2.9	$1.10 \pm 0.23$	$5.7 \pm 1.2$	7.4	$38 \pm 12$
J1151–0004	$7.17 \pm 0.72$	$18.7 \pm 1.9$	24.3	$17.3 \pm 0.2$	$45.2 \pm 0.6$	58.8	$41 \pm 4$
J1518–0137	$0.87 \pm 0.11$	$4.0 \pm 0.5$	5.2	$3.96 \pm 0.16$	$18.1 \pm 0.7$	23.5	$22 \pm 3$
J1522–0044	$1.12 \pm 0.11$	$5.8 \pm 0.6$	7.5	$4.34 \pm 0.14$	$22.6 \pm 0.7$	29.4	$26 \pm 3$
J1226–0118	$0.66 \pm 0.08$	$3.0 \pm 0.4$	3.9	$2.66 \pm 0.13$	$12.0 \pm 0.6$	15.6	$25 \pm 3$

NOTE— Apertures with which we measured the line luminosity are also indicated. The 10% systematic flux uncertainty is included. The last column ( $f_{0.7/2.0}$ ) shows the fraction of  $L'_{\text{CO}(2-1)}$  measured at the central 700 pc relative to that measured at the central 2 kpc.

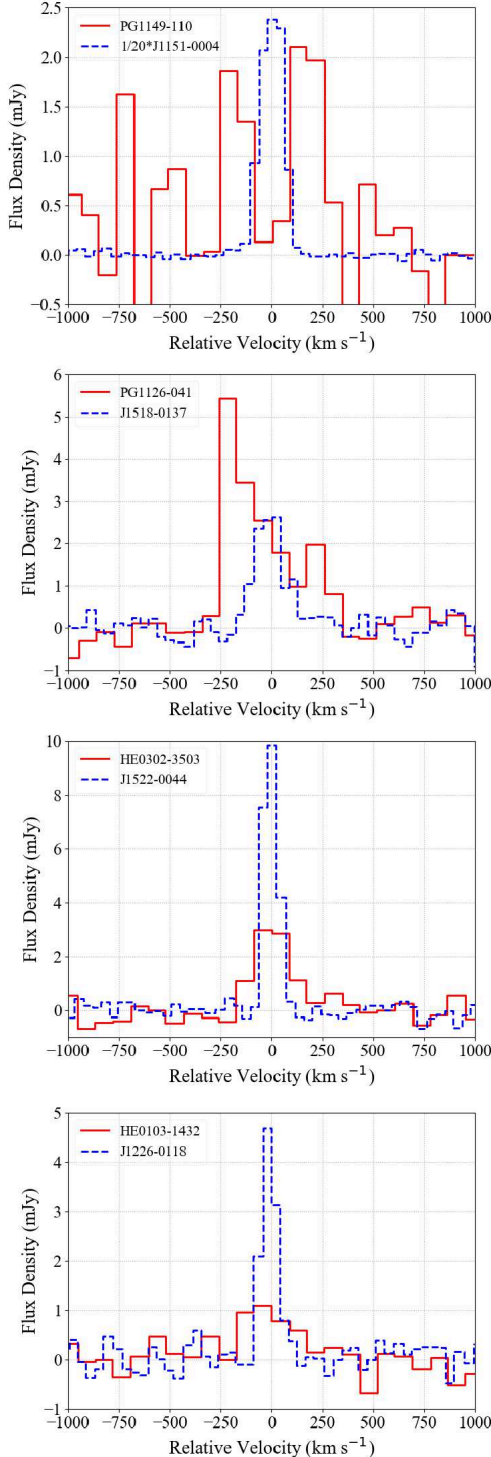


**Figure 4.** The CO(2-1) line spectra of the four pairs of quasars (red-solid line) and the comparison galaxies (blue-dashed line). The spectra in each panel were taken with the apertures matched to the poorer ones in each quasar-galaxy pair. Given the modest signal-to-noise ratio (e.g., PG1149–110) and asymmetric line profile (e.g., PG1126–041), we have not performed Gaussian fittings to these spectra. Note that the flux density of J1151–0004 is scaled by 1/20 to fit into the panel.

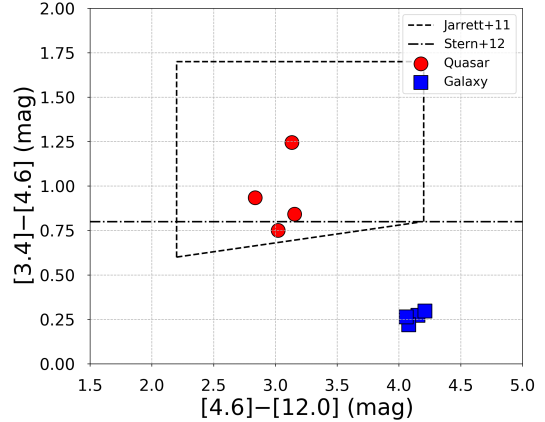


**Figure 5.** *WISE*-based  $4.6 - 12.0 \mu\text{m}$  vs.  $3.4 - 4.6 \mu\text{m}$  color-color diagram. Our target quasars (red circle) and comparison galaxies (blue square) are plotted. The black dashed and dot-dashed lines define the selection criteria of AGNs proposed by [Jarrett et al. \(2011\)](#) and [Stern et al. \(2012\)](#), respectively. Our quasars (galaxies) satisfy the above selection criteria of being a quasar (galaxy).

also found that  $\alpha_{\text{CO}}$  decreases by a factor of  $\sim 2$  from the value averaged over the galaxies. Hence, we adopt  $\alpha_{\text{CO}} = 1.3 M_{\odot} \text{ pc}^{-2} (\text{K km s}^{-1})^{-1}$  in this work, which would have  $\sim 0.4$  dex uncertainty as well. Note that we apply this  $\alpha_{\text{CO}}$  to both the quasar and the comparison galaxy samples, although AGN activity can potentially affect molecular gas properties including gas excitation and chemistry (e.g., [Izumi et al. 2013, 2016b](#)). As a consequence, we obtained  $M_{\text{mol}} = (2.7 - 9.5) \times 10^7 M_{\odot}$  for the quasar sample and  $(3.9 - 24.3) \times 10^7 M_{\odot}$  for the galaxy sample, respectively, in the central 700 pc aperture (Table 3).

### 3.5. Molecular gas mass surface density profiles and circumnuclear gas

A primary goal of this work is to test whether systematically enhanced circumnuclear gas mass surface densities are found in the quasar sample relative to the comparison sample. Figure 6 shows the azimuthally-averaged radial distributions of CO(2–1) integrated intensity<sup>1</sup> and corresponding total molecular gas mass surface density ( $\Sigma_{\text{mol}}$ ) of the four matched pairs measured at the central  $r \leq 2$  kpc. We used MIRIAD ([Sault et al. 1995](#)) task `ellint` to make these plots after matching the physical resolution (i.e., not angular resolution) to the poorer one of each pair. The steps between concentric rings correspond to  $\theta_{\text{maj}}/2$ , where  $\theta_{\text{maj}}$  is the major axis of each 2D Gaussian beam. Note that these profiles are sky projections as we have no robust information

<sup>1</sup> We here describe this quantity in the brightness temperature unit  $I_{\text{CO}(2-1)}$  ( $\text{K km s}^{-1}$ ) for an easy conversion to  $M_{\text{mol}}$ .

about the inclination angles of our targets. However, the inclination angle (projection) effect will impact the final values of  $\Sigma_{\text{mol}}$ . For example, if we assume that the classical AGN torus scheme (Antonucci 1993) is applicable to our quasars, their inclination angle ( $i$ ) may be  $\lesssim 45^\circ - 60^\circ$  (characteristic value for type-1 AGNs, Marin 2014). In this case,  $\Sigma_{\text{mol}}$  could be further reduced by a factor  $\sim 2$  (correction factor =  $\cos i$ ). Future high resolution observations that accurately constrain the gas distribution and/or dynamics are necessary to properly correct this effect both for the quasars and the inactive galaxies.

From Figure 6, the quasar sample shows lower  $\Sigma_{\text{mol}}$  than the comparison sample in three of the four pairs: only PG1126–041 shows higher  $\Sigma_{\text{mol}}$  relative to its comparison galaxy J1518–0137 in the central region. This result would be robust even if we regard the galaxy J1151–0004 to be an anomalous case based on its high  $L'_{\text{CO}(2-1)}$ , as  $\Sigma_{\text{mol}}$  of the paired quasar PG1149–110 is still smaller than the remaining three comparison galaxies at the central  $r \lesssim 500$  pc. Therefore, we do not find *systematically enhanced*  $\Sigma_{\text{mol}}$  in these quasars as compared to the comparison galaxies. This appears to be contradictory to our initial expectation that the gravitational instability at the CND-scale caused by rich amount of gas triggers AGN, which is predicted in various galaxy evolution models (e.g., Hopkins & Quataert 2010), as well as is likely supported by recent observations toward nearby Seyfert galaxies (Izumi et al. 2016a).

Regarding the comparison galaxy sample, their  $\Sigma_{\text{mol}}$  at the central  $r \lesssim 500$  pc are larger than the typical values ( $\sim 50 - 100 M_{\odot}$  pc $^{-2}$ ; measured with the Galactic  $\alpha_{\text{CO}}$ ) found in circumnuclear regions of nearby star-forming galaxies (e.g., Leroy et al. 2008). On the other hand,  $\Sigma_{\text{mol}}$  of our quasars, except for PG1126–041, tend to be comparable ( $\lesssim 70 M_{\odot}$  pc $^{-2}$ ) to that typical value for star-forming galaxies<sup>2</sup>, although the absolute value of  $\Sigma_{\text{mol}}$  critically depends on the adopted  $\alpha_{\text{CO}}$ : the value can increase by, for example,  $\sim 3\times$  when we adopt the Galactic  $\alpha_{\text{CO}}$ . Indeed, recent hydrodynamic simulations predict that  $\alpha_{\text{CO}}$  has a large dispersion (e.g., Wada et al. 2018). As there is no effective way to estimate  $\alpha_{\text{CO}}$  in our targets at this moment, we use the currently adopted value in this work. Future multi- $J$  CO observations can lessen this source of uncertainty.

The lower gas masses in these quasars are also evident on a kpc scale as the CO(2–1) emission of the comparison galaxy sample is brighter and spatially more extended than the quasar sample (Figure 3), although the sensitivity of the line cube is considerably different between the two samples (Table 2). For a practical pur-

pose, we measured  $L'_{\text{CO}(2-1)}$  and  $M_{\text{mol}}$  of the two samples using a common aperture of  $\theta = 2$  kpc (Table 3). The quasar sample shows  $L'_{\text{CO}(2-1)} = (4.5 - 11.6) \times 10^7$  K km s $^{-1}$  pc $^2$  (or  $M_{\text{mol}} = (6 - 15) \times 10^7 M_{\odot}$ )<sup>3</sup>, which is clearly smaller than those of the comparison sample  $L'_{\text{CO}(2-1)} = (12.0 - 45.2) \times 10^7$  K km s $^{-1}$  pc $^2$  (or  $M_{\text{mol}} = (16 - 59) \times 10^7 M_{\odot}$ ). A similar trend was also found over global scales in  $z \sim 1.5$  luminous ( $\log (L_{\text{Bol}}/\text{erg s}^{-1}) > 45 - 46$ ) quasars (Kakkad et al. 2017), and bulge-dominated HE quasars (Husemann et al. 2017).

#### 4. DISCUSSION

We consider four plausible scenarios to explain the molecular gas properties in the central regions of quasar hosts as compared to a matched control sample of star-forming galaxies. All cases need to consider the lower gas content, the dissimilar radial surface brightness profiles and different velocity profiles.

(i) *AGN-driven outflows* – massive outflows in various phases of gas have been observed both in nearby AGNs (e.g., Aalto et al. 2012; Greene et al. 2012; Cicone et al. 2014) and in high redshift quasars (e.g., Nesvadba et al. 2008; Maiolino et al. 2012; Bischetti et al. 2019). Among the multiphase flows (ionized, atomic, and molecular), molecular outflows carry the bulk of the gas masses (e.g., Mizumoto et al. 2019), which are considered to be significant enough to deplete CNDs. If we adopt the positive correlation between AGN luminosity and molecular outflow rate ( $\dot{M}_{\text{H}_2}$ ) derived by Cicone et al. (2014), we expect as high as  $\dot{M}_{\text{H}_2} \simeq 400 M_{\odot}$  yr $^{-1}$  for our quasar sample. Hence the gap of  $M_{\text{mol}}$  between the quasar sample and the comparison sample can be easily reconciled if such molecular outflows have lasted only for  $\sim 1$  Myr, which is a small portion of a typical life-time of quasars ( $\sim 10 - 100$  Myr, Schmidt et al. 2017). We recall that we cannot discern the existence of such outflows with current data given the modest S/N ratios (Figure 4).

A caveat of this scenario is that a large fraction of the CO(2–1) emission of our quasar sample comes from the very central region. For example, the ratio of  $L'_{\text{CO}(2-1)}$  measured with  $\theta = 700$  pc to that measured with  $\theta = 2$  kpc, which is denoted as  $f_{0.7/2.0}$  in Table 3, is systematically higher in the quasar sample ( $\sim 38 - 75\%$ ; average =  $52.6 \pm 7.1\%$ ) than in the comparison sample ( $\sim 22 - 41\%$ ; average =  $27.0 \pm 1.6\%$ ). We may expect an opposite case, i.e., lower central gas concentration in the quasar sample, as AGN-driven outflows basically expel their surrounding gas from inside to outside (King & Pounds 2015). A recent hydrodynamic simulation also suggests that AGNs cause little impact on the surrounding material via winds (Gabor & Bournaud

<sup>2</sup> Note that this is in stark contrast to some previous CO observations toward PG quasars (e.g., Evans et al. 2001, 2006), primarily as those quasars were selected based on their IR brightness.

<sup>3</sup> While we probe  $>$ kpc scales, we continue to use  $\alpha_{\text{CO}} = 1.3 M_{\odot}$  pc $^{-2}$  (K km s $^{-1}$ ) $^{-1}$  for simplicity in this work.

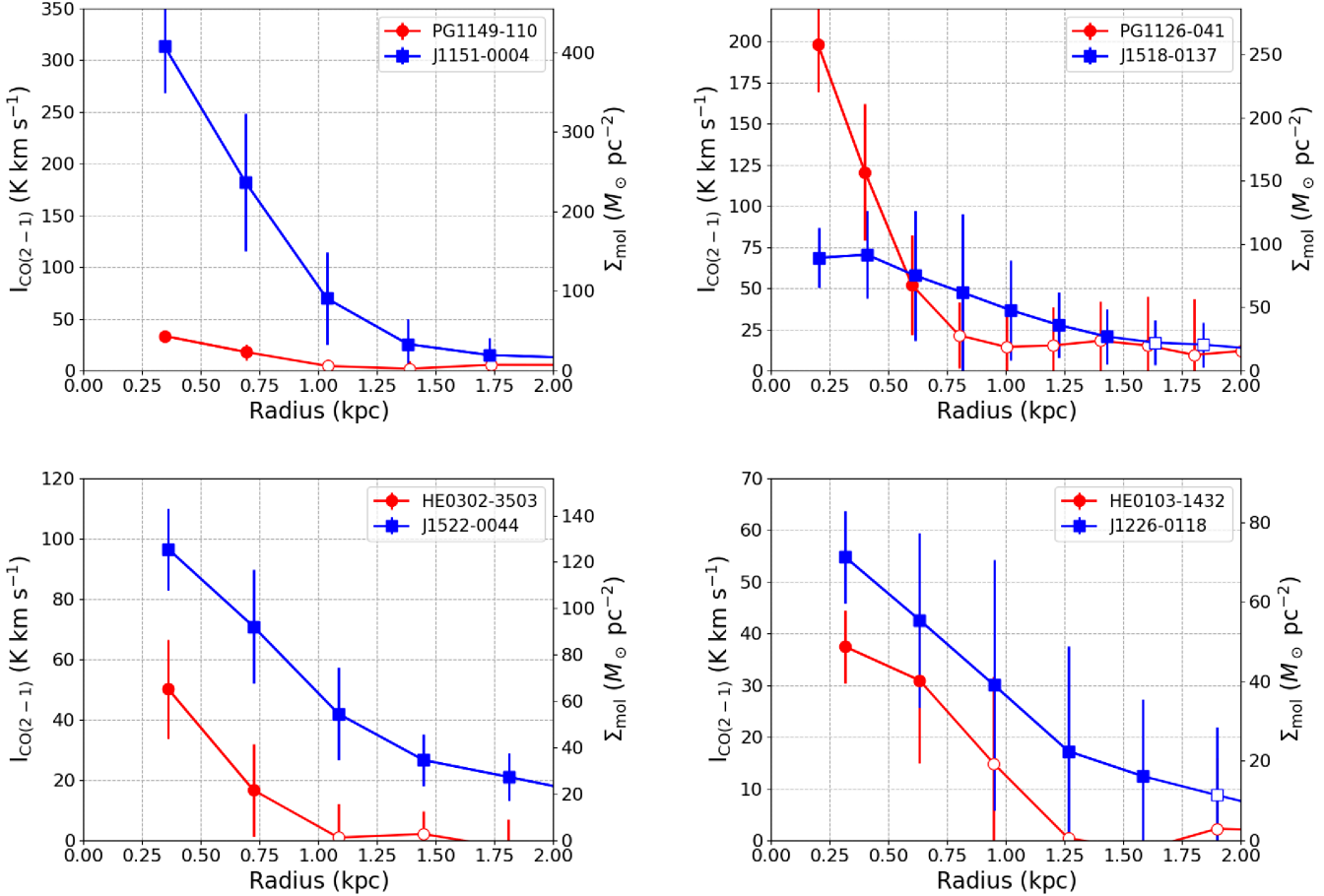


**Figure 6.** Azimuthally-averaged radial distributions of CO(2-1) integrated intensity and corresponding total molecular gas mass surface density of the matched pairs of quasars (red circles) and galaxies (blue squares) measured from each nucleus. Error bars indicate the scatter in each annulus. Open symbols indicate that the values are below  $2\sigma$  of our integrated intensity maps. Note that these are projected profiles on the sky without inclination corrections and the measurements were performed after matching the beam sizes in physical scale.

2014). However, there may be a possibility that the cavity caused by the feedback is much smaller (e.g.,  $< 100$  pc; Hopkins et al. 2016) than our resolutions. Higher resolution observations are definitely needed.

(ii) *Gas-rich minor merger* – the  $M_{\text{mol}}$  we find at the central 700 pc of the quasar sample are of the order of  $10^7 M_{\odot}$ . An average (bulge-scale)  $M_{\star}$ , expected for the quasar sample, is  $\sim 2 \times 10^{10} M_{\odot}$  (Table 1). Hence, a 10:1 minor merger (i.e.,  $M_{\star} = 2 \times 10^9 M_{\odot}$ ) can provide that amount of molecular gas if we assume a typical gas mass fraction of  $\sim$  a few to  $\sim 10$  % for galaxies with  $M_{\star} = 10^9 - 10^{10} M_{\odot}$  (e.g., Morokuma-Matsui & Baba 2015). This scenario is in line with recent observational evidence that major mergers are not the dominant driver of quasar activity at least out to  $z \sim 2$  (e.g., Cisternas et al. 2011; Schawinski et al. 2012; Kocevski et al. 2012; Mechtle et al. 2016). It is particularly noteworthy that if the merging (satellite) galaxy also hosts an SMBH, it can form a binary

system with the primary SMBH, which then causes gravitational instability in the newly formed gas disk (Taniguchi & Wada 1996). Very deep optical imaging observations that can capture evidence of past minor mergers are worth performing, such as done for the nearby Seyfert galaxy NGC 1068 (Tanaka et al. 2017).

(iii) *Time-delay* – Another possible explanation is that a quasar-phase happens during a longer time-scale starburst-phase (e.g., Hopkins 2012). If this is the case, a large portion of the H<sub>2</sub> gas was already consumed by the preceding starburst event. Such time-delay has been predicted not only in galaxy-evolution models including merger-induced ones (e.g., Di Matteo et al. 2005; Hopkins et al. 2008), but also by actual observations (e.g., Davies et al. 2007; Bergvall et al. 2016). Observations suggest that the time-difference between the onsets of the two phases is  $\sim 250 - 500$  Myr (Wild et al. 2010; Schawinski et al. 2010). Hence, our quasar sample could have had another  $\sim 10^9 M_{\odot}$  H<sub>2</sub> gas in the past, if the

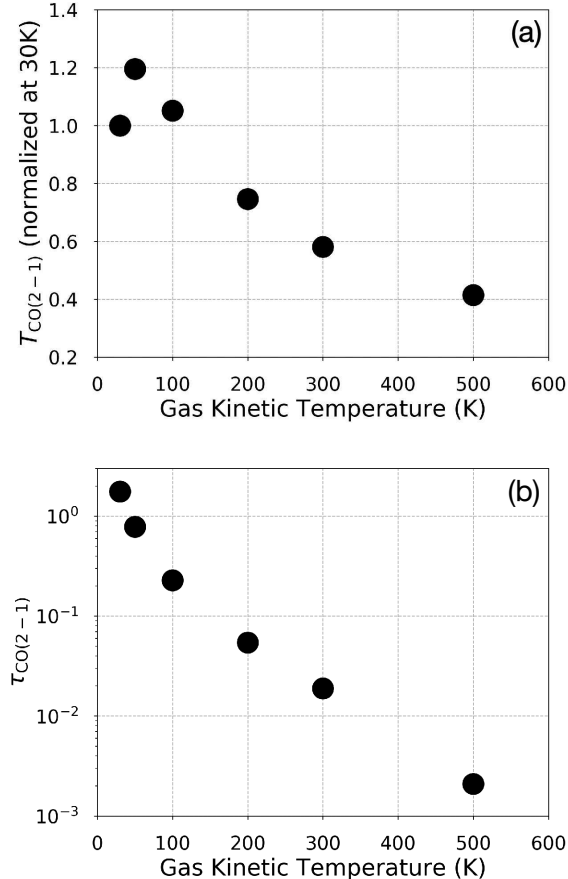


**Figure 7.** Non-LTE radiative transfer modelings of (a) CO(2-1) brightness temperature and (b) its line opacity ( $\tau_{\text{CO}(2-1)}$ ), as a function of gas kinetic temperature ( $T_{\text{kin}}$ ), performed with the RADEX code. The CO(2-1) brightness is normalized by the value at  $T_{\text{kin}} = 30$  K. For simplicity, we only show the results with  $\text{H}_2$  gas density ( $n_{\text{H}_2}$ ) of  $10^5 \text{ cm}^{-3}$  and CO column density-to-velocity width ratio ( $N_{\text{CO}}/dV$ ) of  $2.5 \times 10^{16} \text{ cm}^{-2} (\text{km s}^{-1})^{-1}$ .

currently estimated SFRs (Table 1) have lasted for a 100 Myr. This value can be even larger if the quasars have experienced significant reduction of SFR over their lives. In these cases, we expect significantly greater  $\Sigma_{\text{mol}}$  in the CNDs of our quasars at the time they were actually activated, than the currently observed modest values of  $\Sigma_{\text{mol}}$ .

This time-delay would thus wash out a causality between the CND-scale gas properties including  $\Sigma_{\text{mol}}$  and currently observed quasar activity. Hence, we need to perform a test, like what we did in this work, to AGNs in a much younger phase to better investigate the importance of CND-scale  $\Sigma_{\text{mol}}$  for triggering AGN events. Deeply buried (i.e., dust-obscured) AGNs with high Eddington ratios (e.g., Imanishi et al. 2007; Kawaguchi et al. 2004) would be useful for this test.

Note that there is a suggestion that the amount of gas reaching the nuclear and accretion disk would depend on the initial gas density profile of a galaxy (Cen 2015). The higher  $f_{0.7/2.0}$  in the quasar sample than the comparison sample discovered in this work may still imply the initially-different density profiles we expect.

One thing that needs to be further addressed is the relationship to what has been observed in Seyfert-class objects: at the CND-scale of Seyfert galaxies there is a tight positive correlation between SFR and mass accretion rate onto the AGN (e.g., Diamond-Stanic & Rieke 2012; Esquej et al. 2014), or similarly dense molecular gas mass and accretion rate (Izumi et al. 2016a), while we do not see systematic enhancement in gas amount (or CO(2-1) luminosity as an actual observable here) between the quasar sample and even the non-AGN comparison sample. Regarding this, we speculate that the much higher AGN luminosity in quasars than Seyfert galaxies would explain this difference at some level as discussed in the following.

(iv) *XDR effects* – Owing to the high X-ray flux expected around an AGN, there may form an X-ray dominated region (XDR), in which gas physical and chemical properties are governed by the X-ray irradiation (Maloney et al. 1996; Meijerink & Spaans 2005). While the actual size of the XDR depends on the incident X-ray radiation and gas density, typical values are expected to be several hundred pc (i.e., CND-scale we probed in this work) according to a theoretical work (Schleicher et al. 2010). One notable phenomenon in XDRs is that CO molecules are readily dissociated into C atoms, or ionized to C<sup>+</sup> or higher levels, which reduces CO abundance and consequently CO(2-1) intensity. Another effect in XDRs is that the gas temperature becomes much higher than in star-forming galaxies or photodissociation regions (= PDRs; Meijerink & Spaans 2005). We would therefore expect higher CO excitation in XDRs than in PDRs, which can reduce CO(2-1) line intensity by decreasing the number of CO molecules populating the  $J = 2$  level in AGNs as compared to star-forming galaxies.

To briefly explore the above-mentioned effect of high temperature in XDRs, we performed non local thermodynamic equilibrium (non-LTE) radiative transfer modelings of line intensities by using the RADEX code (van der Tak et al. 2007). In order simply to grasp a qualitative trend, we performed the modelings by fixing the H<sub>2</sub> volume density ( $n_{\text{H}_2}$ ) of  $10^5 \text{ cm}^{-3}$  and the CO column density-to-velocity gradient ratio (this is relevant to line opacity) of  $N_{\text{CO}}/dV = 2.5 \times 10^{16} \text{ cm}^{-2} (\text{km s}^{-1})^{-1}$ , which are characteristic to the CNDs of nearby galaxies (e.g., Izumi et al. 2013; Viti et al. 2014). Throughout the modelings we adopted the cosmic microwave background temperature (2.73 K at  $z = 0$ ) for the background temperature.

Figure 7 shows the resultant values of the CO(2-1) line intensity (brightness temperature) and the line opacity

as a function of the gas kinetic temperature ( $T_{\text{kin}}$ ). Here we modeled cases of  $T_{\text{kin}} = 30, 50, 100, 200, 300$ , and 500 K. There is a trend of reducing the CO(2–1) intensity and the line opacity as increasing  $T_{\text{kin}}$ , as bulk of the CO population is excited to further higher rotational  $J$ -levels. Suppose that the molecular gas temperature is typically  $\lesssim 100$  K in PDRs or star-forming galaxies (Hollenbach & Tielens 1997), whereas it is much higher in XDRs (at least several 100 K; Maloney et al. 1996), we would expect a factor  $> 2 - 3$  reduction in CO(2–1) intensity in AGNs than in star-forming systems even if the total gas mass, gas density, and CO abundance are comparable. Furthermore, the CO abundance is basically lower in XDRs than in PDRs, which further reduces the CO intensity in the former regions. This reduction in CO(2–1) intensity due to the high AGN luminosity of the quasar nucleus itself may consequently make the correlation between the CND-scale CO(2–1) luminosity (we rely on this to derive  $M_{\text{mol}}$ ) and the nuclear activity ambiguous, which would relax the tension with the observations of the lower-luminosity Seyfert galaxies.

These XDR effects have been mainly discussed in nearby Seyfert galaxies (e.g., Izumi et al. 2015), and such discussion is sparse for high redshift objects. However, the effects become stronger with increasing incident X-ray radiation. Now that we are able to probe the central CND-scale molecular gas thanks to the advent of ALMA, we need to carefully consider these effects to properly measure the molecular gas mass in the vicinity of luminous quasar nuclei.

## 5. SUMMARY AND FUTURE PROSPECTS

We have presented high resolution CO(2–1) observations by using ALMA toward 4 pairs of  $z < 0.1$  luminous quasars and normal star-forming galaxies, which are matched in redshift,  $M_*$ , and SFR. Our prime aim is to investigate whether a systematically enhanced gas mass surface density is found at the circumnuclear several  $\times 100$  pc scales of the quasar sample as compared to the inactive comparison sample, which is predicted to be a characteristic initial condition for triggering AGN. Our conclusions are summarized as follows.

- (i) We successfully detected the CO(2–1) emission from all quasars, which show diverse morphology (spiral-arm-like feature, bar-like feature, disk-like feature) in their spatial distributions. The bulk of the line emission we recovered originates from their innermost a few kpc regions. The line emission at the nucleus is brighter in the comparison sample than in the quasar sample in three of the four pairs.
- (ii) The line profile of the quasar sample is clearly broader than the matched comparison sample. Note that, however, we cannot provide a detailed

investigation of the line profiles of the quasar sample (including the search for molecular outflows) given the modest S/N ratios. We also found that two quasars (PG1149–110 and likely PG1126–041) show double-horn like line profiles, which are interpreted as indications of rotating disks.

- (iii) The total molecular gas mass surface density ( $\Sigma_{\text{mol}}$ ) computed from the CO(2–1) line luminosity is accordingly higher in the comparison sample than in the quasar sample at the central sub-kpc regions, in three of the four pairs. Hence, there seems to be no systematic enhancement in  $\Sigma_{\text{mol}}$  in our quasars. This is inconsistent with our initial expectation that  $\Sigma_{\text{mol}}$  is higher in quasars than in comparison galaxies.
- (iv) We discussed four possible explanations for the smaller CO(2–1)-based  $\Sigma_{\text{mol}}$  in the quasar sample, i.e., AGN-driven outflows, gas-rich minor mergers, time-delay between the onsets of a starburst-phase and a quasar-phase, as well as X-ray-dominated region (XDR) effects on the gas chemical abundance and excitation. Although all of these may potentially contribute to the observed low  $\Sigma_{\text{mol}}$  in our quasar sample, we stress the importance of the XDR effects, as we started to probe the CND-scale molecular gas of luminous quasars thanks to the high resolution and sensitivity of ALMA.

The time-delay we discussed in § 4 will wash out a causality between circumnuclear properties and ongoing quasar activities. Hence it is desirable to perform a test, similar to that carried out here, for AGNs in a much younger phase that may maintain the initial conditions to ignite the AGN. As for the XDR, as the actual level of the effects depends on the prevalent physical and chemical conditions of the CND-scale gas, further observations of other transition CO lines as well as other species sensitive to the XDR effects (e.g., atomic carbon line, Meijerink & Spaans 2005; Izumi et al. 2018) are required to obtain a firm conclusion on the importance of CND-scale gas as a fuel reservoir for SMBHs. In addition, for a given  $\Sigma_{\text{mol}}$ , the gas inflow rate will increase with higher stellar mass surface density ( $\Sigma_*$ ) due to stronger torques imposed (e.g., Hopkins & Quataert 2010; Anglés-Alcázar et al. 2017). In future we thus need high resolution stellar mass maps of both quasars and inactive galaxies to measure  $\Sigma_*$  and then construct a better matched sample controlled also by  $\Sigma_*$ . This will be possible after the launch of the *James Webb Space Telescope (JWST)*.

## ACKNOWLEDGMENTS

We thank the anonymous referee for her/his thorough reading and constructive feedback that improved this paper. T.I. appreciates fruitful discussion with M. Imanishi, T. Kawamuro, S. Baba, and D. Nguyen at NAOJ. T.I. and J.D.S. also thank L. Ho, J. Shangguan, and D. Angles-Alcazar for their help and fruitful comments.

This paper makes use of the following ALMA data: ADS/JAO.ALMA#2015.1.00872.S. ALMA is a partnership of ESO (representing its member states), NSF (USA) and NINS (Japan), together with NRC (Canada), MOST and ASIAA (Taiwan), and KASI (Republic of Korea), in cooperation with the Republic of Chile. The Joint ALMA Observatory is operated by ESO, AUI/NRAO and NAOJ.

Funding for SDSS-III has been provided by the Alfred P. Sloan Foundation, the Participating Institutions, the National Science Foundation, and the U.S. Department of Energy Office of Science. The SDSS-III web site is <http://www.sdss3.org/>.

SDSS-III is managed by the Astrophysical Research Consortium for the Participating Institutions of the

SDSS-III Collaboration including the University of Arizona, the Brazilian Participation Group, Brookhaven National Laboratory, Carnegie Mellon University, University of Florida, the French Participation Group, the German Participation Group, Harvard University, the Instituto de Astrofísica de Canarias, the Michigan State/Notre Dame/JINA Participation Group, Johns Hopkins University, Lawrence Berkeley National Laboratory, Max Planck Institute for Astrophysics, Max Planck Institute for Extraterrestrial Physics, New Mexico State University, New York University, Ohio State University, Pennsylvania State University, University of Portsmouth, Princeton University, the Spanish Participation Group, University of Tokyo, University of Utah, Vanderbilt University, University of Virginia, University of Washington, and Yale University.

T.I. was supported by the ALMA Japan Research Grant of NAOJ ALMA Project, NAOJ-ALMA-240. T.I. was also supported by Japan Society for the Promotion of Science (JSPS) KAKENHI Grant Number JP20K14531.

## REFERENCES

Aalto, S., Garcia-Burillo, S., Muller, S., et al. 2012, *A&A*, 537, A44, doi: [10.1051/0004-6361/201117919](https://doi.org/10.1051/0004-6361/201117919)

Anglés-Alcázar, D., Faucher-Giguère, C.-A., Quataert, E., et al. 2017, *MNRAS*, 472, L109, doi: [10.1093/mnrasl/slx161](https://doi.org/10.1093/mnrasl/slx161)

Antonucci, R. 1993, *ARA&A*, 31, 473, doi: [10.1146/annurev.aa.31.090193.002353](https://doi.org/10.1146/annurev.aa.31.090193.002353)

Balbus, S. A., & Hawley, J. F. 1998, *Reviews of Modern Physics*, 70, 1, doi: [10.1103/RevModPhys.70.1](https://doi.org/10.1103/RevModPhys.70.1)

Bayet, E., Gerin, M., Phillips, T. G., & Contursi, A. 2004, *A&A*, 427, 45, doi: [10.1051/0004-6361:20035614](https://doi.org/10.1051/0004-6361:20035614)

Bergvall, N., Marquart, T., Way, M. J., et al. 2016, *A&A*, 587, A72, doi: [10.1051/0004-6361/201525692](https://doi.org/10.1051/0004-6361/201525692)

Bertram, T., Eckart, A., Fischer, S., et al. 2007, *A&A*, 470, 571, doi: [10.1051/0004-6361:20077578](https://doi.org/10.1051/0004-6361:20077578)

Bischetti, M., Maiolino, R., Carniani, S., et al. 2019, *A&A*, 630, A59, doi: [10.1051/0004-6361/201833557](https://doi.org/10.1051/0004-6361/201833557)

Bolatto, A. D., Wolfire, M., & Leroy, A. K. 2013, *ARA&A*, 51, 207, doi: [10.1146/annurev-astro-082812-140944](https://doi.org/10.1146/annurev-astro-082812-140944)

Brinchmann, J., Charlot, S., White, S. D. M., et al. 2004, *MNRAS*, 351, 1151, doi: [10.1111/j.1365-2966.2004.07881.x](https://doi.org/10.1111/j.1365-2966.2004.07881.x)

Carilli, C. L., & Walter, F. 2013, *ARA&A*, 51, 105, doi: [10.1146/annurev-astro-082812-140953](https://doi.org/10.1146/annurev-astro-082812-140953)

Cen, R. 2015, *ApJL*, 805, L9, doi: [10.1088/2041-8205/805/1/L9](https://doi.org/10.1088/2041-8205/805/1/L9)

Cicone, C., Maiolino, R., Sturm, E., et al. 2014, *A&A*, 562, A21, doi: [10.1051/0004-6361/201322464](https://doi.org/10.1051/0004-6361/201322464)

Cisternas, M., Jahnke, K., Inskip, K. J., et al. 2011, *ApJ*, 726, 57, doi: [10.1088/0004-637X/726/2/57](https://doi.org/10.1088/0004-637X/726/2/57)

Cluver, M. E., Jarrett, T. H., Dale, D. A., et al. 2017, *ApJ*, 850, 68, doi: [10.3847/1538-4357/aa92c7](https://doi.org/10.3847/1538-4357/aa92c7)

Davies, R. I., Müller Sánchez, F., Genzel, R., et al. 2007, *ApJ*, 671, 1388, doi: [10.1086/523032](https://doi.org/10.1086/523032)

Di Matteo, T., Springel, V., & Hernquist, L. 2005, *Nature*, 433, 604, doi: [10.1038/nature03335](https://doi.org/10.1038/nature03335)

Diamond-Stanic, A. M., & Rieke, G. H. 2012, *ApJ*, 746, 168, doi: [10.1088/0004-637X/746/2/168](https://doi.org/10.1088/0004-637X/746/2/168)

Eisenstein, D. J., Weinberg, D. H., Agol, E., et al. 2011, *AJ*, 142, 72, doi: [10.1088/0004-6256/142/3/72](https://doi.org/10.1088/0004-6256/142/3/72)

Elbaz, D., Daddi, E., Le Borgne, D., et al. 2007, *A&A*, 468, 33, doi: [10.1051/0004-6361:20077525](https://doi.org/10.1051/0004-6361:20077525)

Ellison, S. L., Patton, D. R., Mendel, J. T., & Scudder, J. M. 2011, *MNRAS*, 418, 2043, doi: [10.1111/j.1365-2966.2011.19624.x](https://doi.org/10.1111/j.1365-2966.2011.19624.x)

Esquej, P., Alonso-Herrero, A., González-Martín, O., et al. 2014, *ApJ*, 780, 86, doi: [10.1088/0004-637X/780/1/86](https://doi.org/10.1088/0004-637X/780/1/86)

Evans, A. S., Frayer, D. T., Surace, J. A., & Sanders, D. B. 2001, *AJ*, 121, 1893, doi: [10.1086/319972](https://doi.org/10.1086/319972)

Evans, A. S., Solomon, P. M., Tacconi, L. J., Vavilkin, T., & Downes, D. 2006, *AJ*, 132, 2398, doi: [10.1086/508416](https://doi.org/10.1086/508416)

Gabor, J. M., & Bournaud, F. 2014, *MNRAS*, 441, 1615, doi: [10.1093/mnras/stu677](https://doi.org/10.1093/mnras/stu677)

García-Burillo, S., Combes, F., Usero, A., et al. 2014, *A&A*, 567, A125, doi: [10.1051/0004-6361/201423843](https://doi.org/10.1051/0004-6361/201423843)

Goulding, A. D., Greene, J. E., Bezanson, R., et al. 2018, *PASJ*, 70, S37, doi: [10.1093/pasj/psx135](https://doi.org/10.1093/pasj/psx135)

Greene, J. E., Zakamska, N. L., & Smith, P. S. 2012, *ApJ*, 746, 86, doi: [10.1088/0004-637X/746/1/86](https://doi.org/10.1088/0004-637X/746/1/86)

Hernquist, L. 1989, *Nature*, 340, 687, doi: [10.1038/340687a0](https://doi.org/10.1038/340687a0)

Hollenbach, D. J., & Tielens, A. G. G. M. 1997, *ARA&A*, 35, 179, doi: [10.1146/annurev.astro.35.1.179](https://doi.org/10.1146/annurev.astro.35.1.179)

Hopkins, P. F. 2012, *MNRAS*, 420, L8, doi: [10.1111/j.1745-3933.2011.01179.x](https://doi.org/10.1111/j.1745-3933.2011.01179.x)

Hopkins, P. F., & Hernquist, L. 2006, *ApJS*, 166, 1, doi: [10.1086/505753](https://doi.org/10.1086/505753)

Hopkins, P. F., Hernquist, L., Cox, T. J., et al. 2006, *ApJS*, 163, 1, doi: [10.1086/499298](https://doi.org/10.1086/499298)

Hopkins, P. F., Hernquist, L., Cox, T. J., & Kereš, D. 2008, *ApJS*, 175, 356, doi: [10.1086/524362](https://doi.org/10.1086/524362)

Hopkins, P. F., & Quataert, E. 2010, *MNRAS*, 407, 1529, doi: [10.1111/j.1365-2966.2010.17064.x](https://doi.org/10.1111/j.1365-2966.2010.17064.x)

Hopkins, P. F., Torrey, P., Faucher-Giguère, C.-A., Quataert, E., & Murray, N. 2016, *MNRAS*, 458, 816, doi: [10.1093/mnras/stw289](https://doi.org/10.1093/mnras/stw289)

Husemann, B., Davis, T. A., Jahnke, K., et al. 2017, *MNRAS*, 470, 1570, doi: [10.1093/mnras/stx1123](https://doi.org/10.1093/mnras/stx1123)

Imanishi, M., Dudley, C. C., Maiolino, R., et al. 2007, *ApJS*, 171, 72, doi: [10.1086/513715](https://doi.org/10.1086/513715)

Izumi, T., Kawakatu, N., & Kohno, K. 2016a, *ApJ*, 827, 81, doi: [10.3847/0004-637X/827/1/81](https://doi.org/10.3847/0004-637X/827/1/81)

Izumi, T., Wada, K., Fukushige, R., Hamamura, S., & Kohno, K. 2018, *ApJ*, 867, 48, doi: [10.3847/1538-4357/aae20b](https://doi.org/10.3847/1538-4357/aae20b)

Izumi, T., Kohno, K., Martín, S., et al. 2013, *PASJ*, 65, 100, doi: [10.1093/pasj/65.5.100](https://doi.org/10.1093/pasj/65.5.100)

Izumi, T., Kohno, K., Aalto, S., et al. 2015, *ApJ*, 811, 39, doi: [10.1088/0004-637X/811/1/39](https://doi.org/10.1088/0004-637X/811/1/39)

—. 2016b, *ApJ*, 818, 42, doi: [10.3847/0004-637X/818/1/42](https://doi.org/10.3847/0004-637X/818/1/42)

Jarrett, T. H., Cohen, M., Masci, F., et al. 2011, *ApJ*, 735, 112, doi: [10.1088/0004-637X/735/2/112](https://doi.org/10.1088/0004-637X/735/2/112)

Kakkad, D., Mainieri, V., Brusa, M., et al. 2017, *MNRAS*, 468, 4205, doi: [10.1093/mnras/stx726](https://doi.org/10.1093/mnras/stx726)

Kauffmann, G., Heckman, T. M., White, S. D. M., et al. 2003, *MNRAS*, 341, 33, doi: [10.1046/j.1365-8711.2003.06291.x](https://doi.org/10.1046/j.1365-8711.2003.06291.x)

Kaviraj, S. 2014, *MNRAS*, 440, 2944, doi: [10.1093/mnras/stu338](https://doi.org/10.1093/mnras/stu338)

Kawaguchi, T., Aoki, K., Ohta, K., & Collin, S. 2004, *A&A*, 420, L23, doi: [10.1051/0004-6361:20040157](https://doi.org/10.1051/0004-6361:20040157)

Kennicutt, R. C., & Evans, N. J. 2012, *ARA&A*, 50, 531, doi: [10.1146/annurev-astro-081811-125610](https://doi.org/10.1146/annurev-astro-081811-125610)

King, A., & Pounds, K. 2015, *ARA&A*, 53, 115, doi: [10.1146/annurev-astro-082214-122316](https://doi.org/10.1146/annurev-astro-082214-122316)

Kocevski, D. D., Faber, S. M., Mozena, M., et al. 2012, *ApJ*, 744, 148, doi: [10.1088/0004-637X/744/2/148](https://doi.org/10.1088/0004-637X/744/2/148)

Kormendy, J., & Ho, L. C. 2013, *ARA&A*, 51, 511, doi: [10.1146/annurev-astro-082708-101811](https://doi.org/10.1146/annurev-astro-082708-101811)

Kormendy, J., & Kennicutt, Robert C., J. 2004, *ARA&A*, 42, 603, doi: [10.1146/annurev.astro.42.053102.134024](https://doi.org/10.1146/annurev.astro.42.053102.134024)

Koss, M. J., Blecha, L., Bernhard, P., et al. 2018, *Nature*, 563, 214, doi: [10.1038/s41586-018-0652-7](https://doi.org/10.1038/s41586-018-0652-7)

Leroy, A. K., Walter, F., Brinks, E., et al. 2008, *AJ*, 136, 2782, doi: [10.1088/0004-6256/136/6/2782](https://doi.org/10.1088/0004-6256/136/6/2782)

Leroy, A. K., Walter, F., Sandstrom, K., et al. 2013, *AJ*, 146, 19, doi: [10.1088/0004-6256/146/2/19](https://doi.org/10.1088/0004-6256/146/2/19)

Lynden-Bell, D., & Rees, M. J. 1971, *MNRAS*, 152, 461, doi: [10.1093/mnras/152.4.461](https://doi.org/10.1093/mnras/152.4.461)

Maiolino, R., Gallerani, S., Neri, R., et al. 2012, *MNRAS*, 425, L66, doi: [10.1111/j.1745-3933.2012.01303.x](https://doi.org/10.1111/j.1745-3933.2012.01303.x)

Maloney, P. R., Hollenbach, D. J., & Tielens, A. G. G. M. 1996, *ApJ*, 466, 561, doi: [10.1086/177532](https://doi.org/10.1086/177532)

Marin, F. 2014, *MNRAS*, 441, 551, doi: [10.1093/mnras/stu593](https://doi.org/10.1093/mnras/stu593)

Mashian, N., Sturm, E., Sternberg, A., et al. 2015, *ApJ*, 802, 81, doi: [10.1088/0004-637X/802/2/81](https://doi.org/10.1088/0004-637X/802/2/81)

McMullin, J. P., Waters, B., Schiebel, D., Young, W., & Golap, K. 2007, Astronomical Society of the Pacific Conference Series, Vol. 376, CASA Architecture and Applications, ed. R. A. Shaw, F. Hill, & D. J. Bell (San Francisco, CA: ASP), 127

Mechtley, M., Jahnke, K., Windhorst, R. A., et al. 2016, *ApJ*, 830, 156, doi: [10.3847/0004-637X/830/2/156](https://doi.org/10.3847/0004-637X/830/2/156)

Meijerink, R., & Spaans, M. 2005, *A&A*, 436, 397, doi: [10.1051/0004-6361:20042398](https://doi.org/10.1051/0004-6361:20042398)

Mihos, J. C., & Hernquist, L. 1994, *ApJL*, 425, L13, doi: [10.1086/187299](https://doi.org/10.1086/187299)

Mizumoto, M., Izumi, T., & Kohno, K. 2019, *ApJ*, 871, 156, doi: [10.3847/1538-4357/aaf814](https://doi.org/10.3847/1538-4357/aaf814)

Morokuma-Matsui, K., & Baba, J. 2015, *MNRAS*, 454, 3792, doi: [10.1093/mnras/stv2227](https://doi.org/10.1093/mnras/stv2227)

Murphy, E. J., Condon, J. J., Schinnerer, E., et al. 2011, *ApJ*, 737, 67, doi: [10.1088/0004-637X/737/2/67](https://doi.org/10.1088/0004-637X/737/2/67)

Nesvadba, N. P. H., Lehnert, M. D., De Breuck, C., Gilbert, A. M., & van Breugel, W. 2008, *A&A*, 491, 407, doi: [10.1051/0004-6361:200810346](https://doi.org/10.1051/0004-6361:200810346)

Netzer, H., Lutz, D., Schweitzer, M., et al. 2007, *ApJ*, 666, 806, doi: [10.1086/520716](https://doi.org/10.1086/520716)

Novak, G. S., Ostriker, J. P., & Ciotti, L. 2011, *ApJ*, 737, 26, doi: [10.1088/0004-637X/737/1/26](https://doi.org/10.1088/0004-637X/737/1/26)

Papadopoulos, P. P., van der Werf, P. P., Xilouris, E. M., et al. 2012, MNRAS, 426, 2601, doi: [10.1111/j.1365-2966.2012.21001.x](https://doi.org/10.1111/j.1365-2966.2012.21001.x)

Rosario, D. J., Trakhtenbrot, B., Lutz, D., et al. 2013, A&A, 560, A72, doi: [10.1051/0004-6361/201322196](https://doi.org/10.1051/0004-6361/201322196)

Saintonge, A., Catinella, B., Tacconi, L. J., et al. 2017, ApJS, 233, 22, doi: [10.3847/1538-4365/aa97e0](https://doi.org/10.3847/1538-4365/aa97e0)

Saito, T., Iono, D., Xu, C. K., et al. 2017, ApJ, 835, 174, doi: [10.3847/1538-4357/835/2/174](https://doi.org/10.3847/1538-4357/835/2/174)

Sanders, D. B., & Mirabel, I. F. 1996, ARA&A, 34, 749, doi: [10.1146/annurev.astro.34.1.749](https://doi.org/10.1146/annurev.astro.34.1.749)

Sandstrom, K. M., Leroy, A. K., Walter, F., et al. 2013, ApJ, 777, 5, doi: [10.1088/0004-637X/777/1/5](https://doi.org/10.1088/0004-637X/777/1/5)

Sault, R. J., Teuben, P. J., & Wright, M. C. H. 1995, Astronomical Society of the Pacific Conference Series, Vol. 77, A Retrospective View of MIRIAD, ed. R. A. Shaw, H. E. Payne, & J. J. E. Hayes (San Francisco, CA: ASP), 433

Schawinski, K., Dowlin, N., Thomas, D., Urry, C. M., & Edmondson, E. 2010, ApJL, 714, L108, doi: [10.1088/2041-8205/714/1/L108](https://doi.org/10.1088/2041-8205/714/1/L108)

Schawinski, K., Koss, M., Berney, S., & Sartori, L. F. 2015, MNRAS, 451, 2517, doi: [10.1093/mnras/stv1136](https://doi.org/10.1093/mnras/stv1136)

Schawinski, K., Simmons, B. D., Urry, C. M., Treister, E., & Glikman, E. 2012, MNRAS, 425, L61, doi: [10.1111/j.1745-3933.2012.01302.x](https://doi.org/10.1111/j.1745-3933.2012.01302.x)

Schleicher, D. R. G., Spaans, M., & Klessen, R. S. 2010, A&A, 513, A7, doi: [10.1051/0004-6361/200913467](https://doi.org/10.1051/0004-6361/200913467)

Schmidt, M., & Green, R. F. 1983, ApJ, 269, 352, doi: [10.1086/161048](https://doi.org/10.1086/161048)

Schmidt, T. M., Worseck, G., Hennawi, J. F., Prochaska, J. X., & Crighton, N. H. M. 2017, ApJ, 847, 81, doi: [10.3847/1538-4357/aa83ac](https://doi.org/10.3847/1538-4357/aa83ac)

Schulze, A., & Wisotzki, L. 2010, A&A, 516, A87, doi: [10.1051/0004-6361/201014193](https://doi.org/10.1051/0004-6361/201014193)

Schulze, A., Wisotzki, L., & Husemann, B. 2009, A&A, 507, 781, doi: [10.1051/0004-6361/200912730](https://doi.org/10.1051/0004-6361/200912730)

Scoville, N. Z., Frayer, D. T., Schinnerer, E., & Christopher, M. 2003, ApJL, 585, L105, doi: [10.1086/374544](https://doi.org/10.1086/374544)

Shangguan, J., Ho, L. C., Bauer, F. E., Wang, R., & Treister, E. 2020, ApJS, 247, 15, doi: [10.3847/1538-4365/ab5db2](https://doi.org/10.3847/1538-4365/ab5db2)

Shankar, F., Weinberg, D. H., & Miralda-Escudé, J. 2009, ApJ, 690, 20, doi: [10.1088/0004-637X/690/1/20](https://doi.org/10.1088/0004-637X/690/1/20)

Shlosman, I., Begelman, M. C., & Frank, J. 1990, Nature, 345, 679, doi: [10.1038/345679a0](https://doi.org/10.1038/345679a0)

Silverman, J. D., Kampczyk, P., Jahnke, K., et al. 2011, ApJ, 743, 2, doi: [10.1088/0004-637X/743/1/2](https://doi.org/10.1088/0004-637X/743/1/2)

Solomon, P. M., & Vanden Bout, P. A. 2005, ARA&A, 43, 677, doi: [10.1146/annurev.astro.43.051804.102221](https://doi.org/10.1146/annurev.astro.43.051804.102221)

Stern, D., Assef, R. J., Benford, D. J., et al. 2012, ApJ, 753, 30, doi: [10.1088/0004-637X/753/1/30](https://doi.org/10.1088/0004-637X/753/1/30)

Tanaka, I., Yagi, M., & Taniguchi, Y. 2017, PASJ, 69, 90, doi: [10.1093/pasj/psx100](https://doi.org/10.1093/pasj/psx100)

Taniguchi, Y. 1999, ApJ, 524, 65, doi: [10.1086/307814](https://doi.org/10.1086/307814)

Taniguchi, Y., & Wada, K. 1996, ApJ, 469, 581, doi: [10.1086/177807](https://doi.org/10.1086/177807)

Urrutia, T., Lacy, M., & Becker, R. H. 2008, ApJ, 674, 80, doi: [10.1086/523959](https://doi.org/10.1086/523959)

van der Tak, F. F. S., Black, J. H., Schöier, F. L., Jansen, D. J., & van Dishoeck, E. F. 2007, A&A, 468, 627, doi: [10.1051/0004-6361:20066820](https://doi.org/10.1051/0004-6361:20066820)

Vestergaard, M., & Peterson, B. M. 2006, ApJ, 641, 689, doi: [10.1086/500572](https://doi.org/10.1086/500572)

Viti, S., García-Burillo, S., Fuente, A., et al. 2014, A&A, 570, A28, doi: [10.1051/0004-6361/201424116](https://doi.org/10.1051/0004-6361/201424116)

Wada, K., Fukushige, R., Izumi, T., & Tomisaka, K. 2018, ApJ, 852, 88, doi: [10.3847/1538-4357/aa9e53](https://doi.org/10.3847/1538-4357/aa9e53)

Wild, V., Heckman, T., & Charlot, S. 2010, MNRAS, 405, 933, doi: [10.1111/j.1365-2966.2010.16536.x](https://doi.org/10.1111/j.1365-2966.2010.16536.x)

Wisotzki, L., Christlieb, N., Bade, N., et al. 2000, A&A, 358, 77, <https://arxiv.org/abs/astro-ph/0004162>

Wright, E. L., Eisenhardt, P. R. M., Mainzer, A. K., et al. 2010, AJ, 140, 1868, doi: [10.1088/0004-6256/140/6/1868](https://doi.org/10.1088/0004-6256/140/6/1868)

**Table A1.** Properties of the quasar and the galaxy excluded from our test

Name	R.A. (ICRS)	Decl. (ICRS)	$z_{\text{opt}}$	Scale (kpc/‘‘)	$\log \left( \frac{M_{\text{BH}}}{M_{\odot}} \right)$	$\log \left( \frac{L_{\text{bol}}}{\text{erg/s}} \right)$	$\log \left( \frac{M_{\star}}{M_{\odot}} \right)$	$\log \left( \frac{SFR}{M_{\odot}/\text{yr}} \right)$
HE0205–2408	02:07:47.755	–23:54:10.62	0.076	1.44	8.33	45.6	10.69	1.25
J0042–0940	00:42:27.540	–09:40:36.25	0.077	1.46	–	–	10.75	$\sim -2^{\dagger}$

NOTE—<sup>†</sup>This is a SFR measured with a 3‘‘ fiber aperture. As this SFR is significantly smaller than that of the paired quasar HE0205–2408, we excluded this galaxy, and consequently this pair, from the sample for our test.

## APPENDIX

### A. PROPERTIES OF ONE QUASAR-GALAXY PAIR EXCLUDED FROM OUR TEST

We excluded one quasar HE0205–2408 and a galaxy J0042–0940, which were initially paired (Table A1). The reason for this exclusion is the mismatched SFR: the MPA-JHU galaxy catalog shows that the galaxy J0042–0940 has  $\log(\text{SFR}/M_{\odot} \text{ yr}^{-1}) \sim 1.2$  when it is measured over the galaxy-scale, which is comparable to the SFR estimated for the quasar HE0205–2408. However, the SFR of J0042–0940 measured with a 3‘‘ fiber aperture is only  $\log(\text{SFR}/M_{\odot} \text{ yr}^{-1}) \sim -2$ , which is orders of magnitude smaller than that estimated at the galaxy-scale. The *WISE* photometry (§ 3.2) also indicates that  $\log(\text{SFR}/M_{\odot} \text{ yr}^{-1}) \sim -2$  (W3 band magnitude = 12.7 mag). Hence, we suppose that there is an unexpected error in the SFR estimation at the galaxy-scale, and the very small SFR measured with the fiber aperture is the correct one for this galaxy. Since HE0205–2408 and J0042–0940 do not compose a well-matched pair any more, we excluded this pair from our discussion.

We observed these objects with ALMA and analyzed the data in the same manner as described in § 2. The obtained synthesized beam sizes for the CO(2–1) cube and the continuum image are, 0‘‘.39  $\times$  0‘‘.29 (P.A. = 87.7°) and 0‘‘.37  $\times$  0‘‘.29 (P.A. = 86.6°) for HE0205–2408 and 0‘‘.43  $\times$  0‘‘.32 (P.A. = 79.3°) and 0‘‘.42  $\times$  0‘‘.31 (P.A. = 79.4°) for J0042–0940, respectively. With the natural weighting, we obtained  $1\sigma$  sensitivity of 0.30 mJy beam $^{-1}$  ( $dV \sim 87 \text{ km s}^{-1}$ ) and 0.20 mJy beam $^{-1}$  ( $dV \sim 44 \text{ km s}^{-1}$ ) for the CO(2–1) cubes of HE0205–2408 and J0042–0940, respectively. The CO(2–1) emission was undetected in both objects (Figure A1): the corresponding  $3\sigma$  upper limits are 0.33 Jy km s $^{-1}$  (integrated velocity width = 700 km s $^{-1}$ ) and 0.07 Jy km s $^{-1}$  (integrated velocity width = 450 km s $^{-1}$ ), both of which are measured at the central 700 pc region. On the other hand, we detected the continuum emission significantly in HE0205–2408 ( $1\sigma = 52 \mu\text{Jy beam}^{-1}$ ; max = 2.63 mJy beam $^{-1}$ ), while it is not detected in J0042–0940 ( $1\sigma = 20 \mu\text{Jy beam}^{-1}$ ). Given the deficit of molecular gas around the nucleus, we consider that the bulk of this continuum emission of HE0205–2408 to be of non-thermal origin.

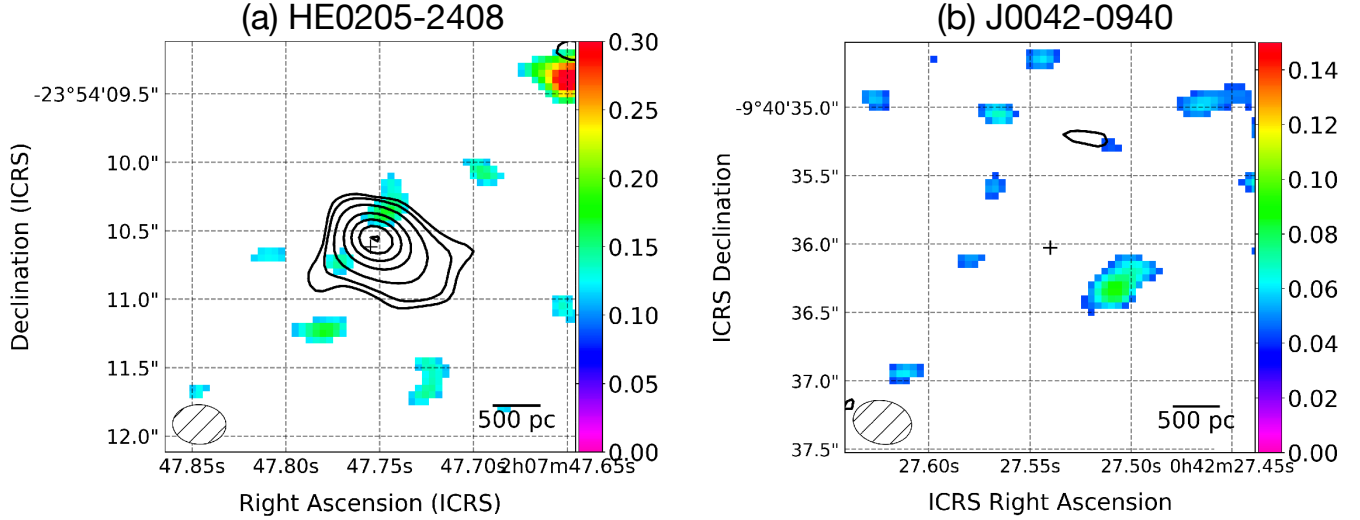


**Figure A1.** Velocity-integrated intensity maps of the CO(2–1) line emission (in the unit of  $\text{Jy beam}^{-1} \text{ km s}^{-1}$ ) of the central  $3''$  region of a quasar (a) HE0205–2408 and a comparison galaxy (b) J0042–0940. The  $1\sigma$  sensitivity is 0.074 and 0.028  $\text{Jy beam}^{-1} \text{ km s}^{-1}$  for (a) and (b), respectively. These CO(2–1) maps are clipped at  $1.5\sigma$  level to enhance the clarity. The central plus signs indicate the location of the quasar nuclei or galactic centers. Also plotted contours indicate the underlying continuum emission distributions drawn at  $-3, 3, 5, 10, 20, 30, 40$ , and  $50\sigma$  (see text for  $1\sigma$  values).